Evolution of Ge/Si(001) islands during Si capping at high temperature

G. Capellini,[a] M. De Seta, L. Di Gaspare, and F. Evangelisti
Università Roma Tre, Via della Vasca Navale 84, I-00146 Roma, Italy

F. d'Acapito
CNR-INFM-OGG c/o European Synchrotron Radiation Facility GILDA CRG, 6, Rue Jules Horowitz, F-38043 Grenoble, France

(Received 1 July 2005; accepted 1 November 2005; published online 16 December 2005)

We discuss the effect of the deposition of a Si cap layer on the composition and morphological properties of Ge(Si)/Si(001) self-assembled islands deposited by chemical vapor deposition at 750 °C. The morphological evolution of the island shape was investigated by means of atomic force microscopy and the actual island composition has been measured by means of x-ray photoemission spectroscopy and x-ray absorption spectroscopy techniques. At an early stage of Si capping, Si atoms are incorporated in the island layer. As a consequence, we observe a reverse Stranski-Krastanov growth dynamics in agreement with the volume-composition stability diagram proposed for domes, pyramids, and prepyramids in the Ge_xSi_{1-x}/Si(100) system. We find that the island burying begins when the Ge average composition reaches the value $x=0.28$. Once the islands are buried under a thin silicon layer their composition is unaffected by subsequent silicon deposition. We conclude that strain relief, rather than thermal diffusion, is the main driving force for the observed Ge-Si alloying. © *2005 American Institute of Physics*. [DOI: 10.1063/1.2141652]

INTRODUCTION

Ge-on-Si self-assembled islands have attracted a wide interest since they could potentially be exploited in the fabrication of new devices compatible with the well-developed Si technology.[1] Most of the proposed devices are based on Ge island multilayers embedded in a Si matrix that provides the confining potential-barrier for charge carriers.[2–4] The optical and electronic properties of the resulting devices depend strongly on the island shape and composition, which, in turn, are influenced by the deposition conditions, with the deposition temperature playing a major role.[5–7]

More recently, it became evident that, depending on the deposition conditions, the Si-cap-layer deposition process can bring about a substantial variation in shape and size of previously deposited islands.[8] Rastelli *et al.*[9] have shown that the deposition of a Si amount as small as 0.5 Si monolayers at 450 °C determines a dramatic island shape modification. Upon increasing the amount of deposited Si, the multifaceted strained domes transform into square-based pyramids, with an increase of the base area and a simultaneous decrease of their height. Cui *et al.*[10] and Lee *et al.*[11] have shown that, during Si capping at 600 °C and 680 °C, respectively, this dome-to-pyramid shape transition is followed by the formation of "ring" structures. It was demonstrated that in order to preserve the island shape and composition a very low capping temperature (300 °C) must be used.[8]

The island-shape evolution was explained in terms of Si-Ge intermixing, occurring during the capping process (and after, if the sample is kept at high temperature) and mass transport from the top to the side surface of the islands. However, a direct measurement of the island composition at different stages of the cap-layer deposition is not yet performed.

In a previous paper[5] we have demonstrated that x-ray photoemission spectroscopy (XPS), complemented by atomic force microscopy (AFM) characterization, can be used to assess the Ge content in a layer close to the surface. In this method, the experimental Ge($3d$)/Si($2p$) XPS peak intensity ratios are fitted with the theoretical photoemission intensities calculated with the help of the measured sample morphology and using the Ge content as fitting parameter.

Furthermore, x-ray absorption spectroscopy (XAS) was used in order to monitor the evolution of the first coordination shell of the Ge atoms as a function of the equivalent thickness of the Ge island layer.[12] XAS studies have demonstrated the effectiveness of this technique for determining quantitatively the intermixing level in the case of Ge dots deposited on Si (Ref. 12) and of thin continuous Ge films deposited[13] or embedded in Si.[14,15] The main advantage of this technique is twofold. It determines directly the chemical composition from the number of nearest neighbors around the Ge atom. The signal intensity has no appreciable depth dependence (whereas the opposite is true for XPS) for the typical layer thickness involved in this study.

Our purpose in this paper is to determine quantitatively, by means of a combined use of AFM, XPS, and XAS techniques, composition, shape, and size changes of Ge/Si islands during the Si-cap deposition at a growth temperature as high as 750 °C.

EXPERIMENTAL DETAILS

The samples were deposited in an ultrahigh vacuum chemical vapor deposition (UHV-CVD) reactor whose base pressure was in the low 10^{-10} Torr range. The Si(100) sub-

[a]Author to whom correspondence should be addressed; electronic mail: capellini@fis.uniroma3.it

strates, after a preliminary outgassing, were cleaned at 1100 °C in H_2 atmosphere. Subsequently, a 500 nm-thick Si buffer layer was grown from high purity silane at a deposition temperature of 800 °C. Then a Ge island layer of 1.3 -nm equivalent thickness was deposited at $T=750$ °C with a germane pressure of 0.4 mTorr and no carrier gas.

In order to investigate the evolution of the Ge islands during the Si overgrowth, the islands were capped with Si layers having thickness ranging from 1 to 33 nm. The growth rate was 1 Å/s, the silane pressure 0.7 mTorr, and the deposition temperature $T=750$ °C.

The morphological characterization of the samples was performed by means of an ambient Veeco CP-II Atomic Force Microscope system, operating in contact mode using high aspect ratio tips with a minimum nominal tip radius of 5 nm (Ultralever™). Finite tip-size convolution effects were taken in to account in the analysis.

XPS measurements were performed *in situ* using a monochromatic Al $K\alpha$ source and a concentric hemispherical analyzer (CHA). The intensity of the Ge($3d$) and Si($2p$) core levels were monitored as a function of the thickness of the silicon cap layer. Since the corresponding photoelectrons have the same escape depth (~2.4 nm), the core level intensity ratio depends just on the actual sample composition and morphology.[5]

XAS measurements[16] at the Ge K edge ($E=11\,103$ eV) were carried out at the GILDA CRG beamline of the European Synchrotron Radiation Facility (ESRF).[17] The monochromator was equipped with a pair of Si(311) crystals operating in dynamical focusing mode.[18] The harmonic rejection was achieved by using a pair of Pd coated mirrors with a cutoff energy $E\approx 21$ keV. Data were collected at liquid nitrogen temperature and in fluorescence mode by using a single element high purity Ge detector. The samples were mounted in a vibrating sample holder in order to minimize the spectral distortions induced by coherent scattering in the substrate. For each sample, four spectra were collected and averaged. As model compounds the spectra of crystalline Ge and Ge diluted in Si were measured in transmission and fluorescence mode, respectively. The spectrum of Ge oxide was taken from the International XAFS Society database.[19]

RESULTS

Surface morphology

In Fig. 1 we report the AFM images of samples obtained by depositing Si layers of different equivalent thickness θ_{Si} on nominally identical Ge island layers.

The islands in samples with $\theta_{Si}<8$ nm have been quantitatively analyzed. For each sample about 4000 individual islands were measured by using a computer aided procedure. In Fig. 2 we report the outcome of this analysis as a function of the Si equivalent thickness. The average values of the base area, volume, height, and aspect ratio are displayed. The standard deviations of the resulting statistical distributions are shown as error bars. In the statistical analysis we applied a cutoff procedure which neglects the smallest features relative to the shrinking pyramids (see hereafter).

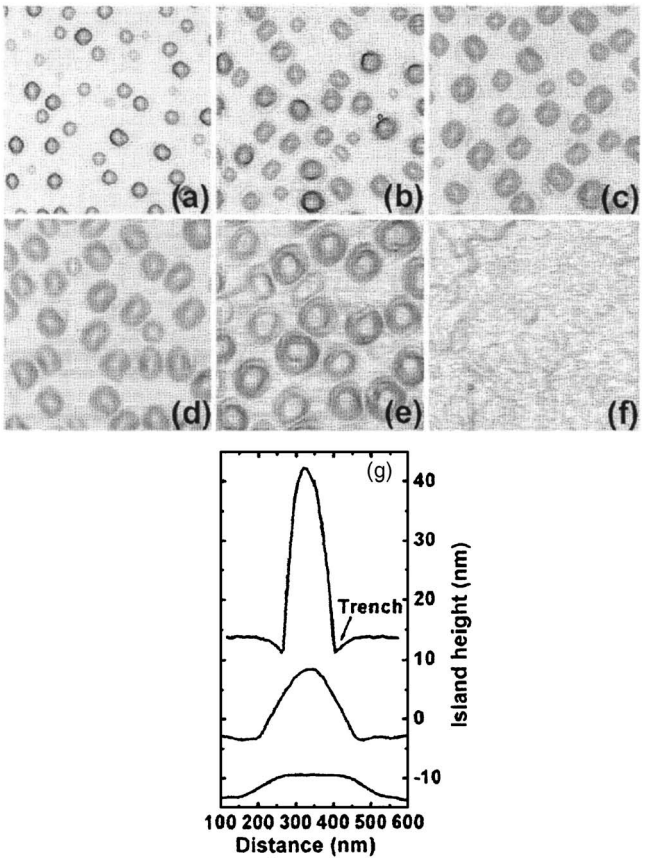

FIG. 1. 2 μm$\times$2 μm AFM images displayed in differential mode describing the evolution of a Ge island layer under silicon capping: cap-layer thickness (a) $\theta_{Si}=0$, (b) 1, (c) 2.7, (d) 4.5, (e) 7.5, (f) 33 nm. In panel (g) we display a [010] line profile of typical islands at different capping stage: top $\theta_{Si}=0$ nm, mid $\theta_{Si}=2.7$ nm, bottom $\theta_{Si}=7.5$ nm.

In the as-deposited Ge/Si sample [Fig. 1(a)], we found a coexistence of pyramids and strained domes.[20] However, the strained domes are the vast majority (82%) of the island population, corresponding to a density of 8.6×10^8 domes/cm^2. A typical-dome height profile along the [010] direction, evidencing the multifaceted shape and the presence of intermixing-induced trenches surrounding the

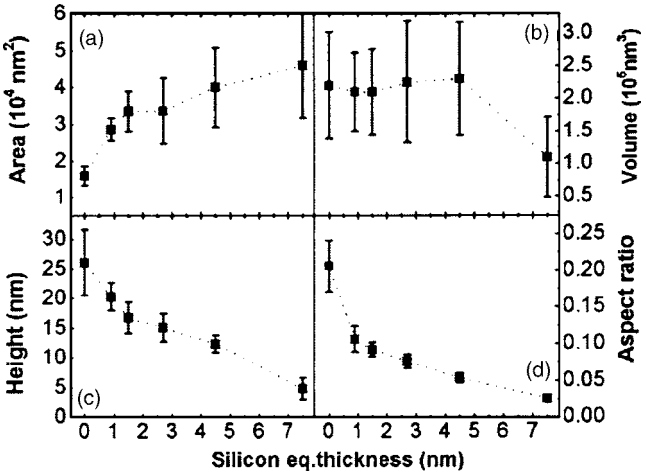

FIG. 2. (a) Average area, (b) average volume, (c) average height, and (d) average aspect ratio of the islands as a function of the deposited silicon equivalent thickness.

dome,[21] is shown in panel (g) (top curve) of Fig. 1. Owing to the relatively high degree of intermixing the island base width, defined as square root of the island projected area, is $b=120$ nm and island height is $h\approx 25$ nm.[6]

The silicon capping in our experimental conditions results in a remarkable morphological evolution of the islands already at very small coverage. Indeed, in the sample capped by the thinnest silicon layer [$\theta_{Si}=1$ nm, Fig. 1(b)] most of the strained domes have become pyramids or elongated pyramids (similar to hut cluster), with sides oriented along the [010] equivalent directions. A further Si deposition ($\theta_{Si}=2.7$ nm) entails the complete disappearance of the strained domes [Fig. 1(c)].

As can be observed in Fig. 2, the average area of the islands increases by a factor of ~2, the average height h decreases appreciably and the aspect ratio $\alpha=h/b$ abruptly drops to the value $\alpha=0.1$, characteristic of the square pyramids with (105) facets.[9,20] This observation is confirmed by the height profile along the [010] direction of a typical pyramid reported in the midcurve of Fig. 1(g). The measured facet angle is 11° as expected for a (105) facet. Moreover the profile evidences that the trenches, which are present around the strained domes, disappear upon shape transformation from dome to pyramid.

A subsequent Si deposition [$\theta_{Si}=4.5$ nm, Fig. 1(d)] leads to a "rounding off" of the pyramid square base. For $\theta_{Si}\geqslant 7.5$ nm [Fig. 1(e)] the islands lose their pyramidal shape: well-defined lateral facets disappear while a (100) facet develops on top, as shown in Fig. 1(g) (bottom curve). We will refer to these islands as prepyramids.

A further decrease of height and aspect ratio (Fig. 2) occurs with a noticeable reduction of the volume as measured by the AFM. The island density at this stage of the capping process is equal, within the statistical error, to the density of the strained domes of the uncapped sample. This means that the strained pyramids observed on the uncapped sample surface, which amounted to ~20% of the total number of islands, are dissolved and/or incorporated in larger islands as the capping proceeds.

For larger deposited θ_{Si}, the sample morphology becomes moundlike, without well defined morphological features and, eventually, evolves toward a fully bidimensional growth of the silicon cap layer (layer by layer). The AFM-measured surface roughness (RMS) decreases from $r=1.4$ nm ($\theta_{Si}=10$ nm) to $r=0.3$ nm [$\theta_{Si}=33$ nm, Fig. 1(f)].

Composition

In Fig. 3 we report the ratio ρ between the intensities of the XPS signal from Ge($3d$) and the Si($2p$) core level as a function of the Si cap-layer equivalent thickness θ_{Si}.

ρ slightly decreases for increasing θ_{Si} in the 0–4.5 nm range, i.e., in the range where well defined pyramids are still present with an apparent constant volume. These data show that capping with thin Si layers entails an effective atomic intermixing, characterized by a redistribution of Ge atoms rather than a burial of the Ge island layer. As already reported, missing dimer rows in the wetting layer[22] and trenches surrounding the island[23] can act as channels for silicon migration inside the Ge(Si) island layer.

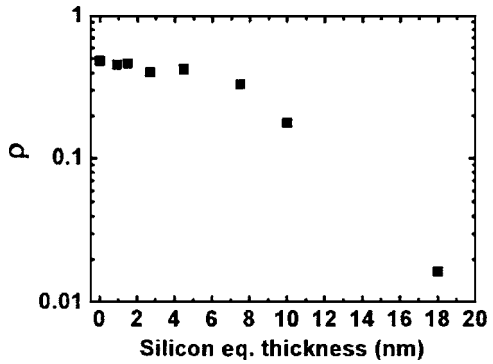

FIG. 3. Ratio ρ between the intensities of the XPS signal from Ge($3d$) and the Si($2p$) core levels, as a function of the Si cap-layer equivalent thickness θ_{Si}.

For thicker silicon deposition, we observe in Fig. 3 the exponential decay of the ratio ρ typical of the presence of a silicon layer on top of the buried regions containing germanium.

In order to determine quantitatively the Ge content we have applied the method reported in Ref. 5 to those samples where the islands are not yet buried by the silicon layer and the AFM images show a well defined island shape ($\theta_{Si}<4.5$ nm). The obtained values of the average Ge content x as a function of the Si equivalent thickness are reported in Fig. 4 (open squares). Notice that, because of the relatively small escape depth of photoelectrons (2.4 nm) compared to the island height (13–25 nm), this value represents the actual Ge content in the wetting layer and in the outmost part of the Ge islands.

We point out that the variation of the germanium content, from $x=0.46$ to $x=0.3$, is not in contrast with a nearly constant ratio of the germanium versus silicon photoemission current given the observed evolution of the sample morphology. As a matter of fact, the enlargement of the island base width and the increase of the wetting layer thickness reduce the contribution of the silicon substrate to the measured photoemission current.

More direct information on the intermixing process at every Si equivalent thickness can be obtained by looking at

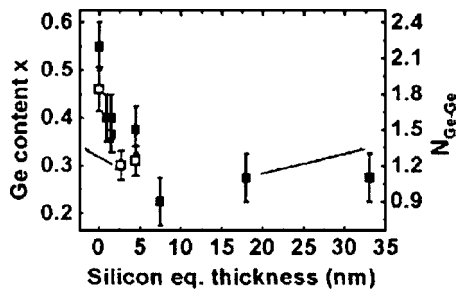

FIG. 4. Average Ge content x as a function of the silicon cap-layer thickness, as measured by the AFM/XPS technique (open symbols left axis) and average Ge-Ge coordination number $N_{Ge\text{-}Ge}$ (solid symbols right axis) as obtained by XAS measurements. The scales on the right and left axis have been matched using the relationship $x=N_{Ge\text{-}Ge}/4$.

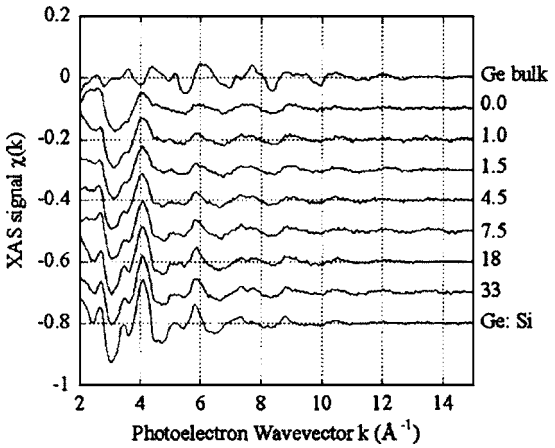

FIG. 5. XAS spectra of the samples for increasing Si-cap layer equivalent thickness (displayed along the right axis). The spectra of the bulk Ge and Ge diluted in Si are also shown for comparison.

the Ge average coordination by means of XAS.[1,12] Therefore, we can obtain the average composition of the island layer (islands and the wetting layer).

The raw x-ray absorption fine structure function $\chi(k)$ (Ref. 24) for the samples investigated is shown in Fig. 5, whereas the related Fourier transform (FT) is shown in Fig. 6. The Ge-Si intermixing is already evident, at a qualitative level, in the raw spectra of Fig. 5. All sample spectra exhibit a close similarity with that of the diluted-Ge model sample. In particular we notice that in the crystalline Ge spectrum a minimum of the oscillation is observed at 4 Å^{-1}, where a maximum in the diluted-Ge sample is present.

This is due to the different phase and frequency of the oscillations due to Si or Ge backscatterers. The samples exhibit a smooth transition from just a small peak at 4 Å^{-1} in the uncapped sample (higher Ge content) to a clearly evident peak in samples with completely buried islands ($\theta_{Si} > 5$ nm, higher Si content). This behavior is reflected in the Fourier-transformed spectra (Fig. 6): indeed crystalline Ge or Ge diluted in Si signals exhibit first coordination shell peaks

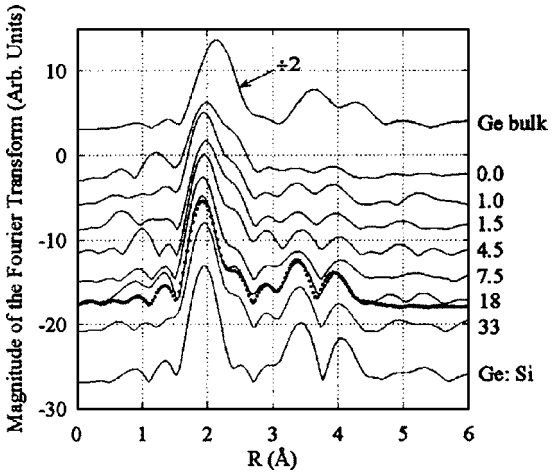

FIG. 6. Fourier transforms of the XAS spectra for increasing equivalent Si-cap layer thickness (displayed along the right axis). The transforms were carried out in the common interval $k=[2.8,\ldots,11]$ Å^{-1} with a Hanning window and a k^3 weight. An example of the typical fit is shown for sample having an 18-nm-thick cap layer (dots).

quite symmetric at different apparent distances whereas intermixed samples exhibit a double peak due to both the Ge-Si ($R \approx 2$ Å) and Ge-Ge contributions (higher distances R). The latter term decreases noticeable in passing from the uncapped sample to the capped ones, in agreement with the considerations made on the $\chi(k)$ spectra.

A quantitative data analysis of the spectra was carried out by generating theoretical signals with the Feff 8.1 code[25] and fitting the experimental data with the FEFFIT code.[26] Calculations used the Hedin-Lundqvist description of the exchange-correlation part of the potential and were based on clusters derived from the structure of crystalline Ge (No. 1) and GeO_2 (No. 2).[27] The cluster related to the Ge diluted in Si (No. 3) was created starting from a Si structure, introducing a substitutional Ge atom and then minimizing the strain energy (bond stretching plus bond bending)[28] by relaxing the positions of the first and second neighbors around Ge. From cluster Nos. 1, 2, and 3 the first shell theoretical signals for respectively the Ge-Ge, Ge-O, and Ge-Si pairs were calculated.

The fits were carried out on the data backtransformed in the range $R=[1.0-2.7]$ Å.

The full model employed to analyze the samples consisted in two independent phases: oxide and Ge dispersed in Si with associated weights x_{ox} and $(1-x_{ox})$. The former, added to account for the native oxide that forms upon air exposure, contains a Ge-O contribution whereas the latter contains Ge-Ge plus Ge-Si contributions. It is worth noting that the oxide phase was detectable only in samples with no or low Si capping. The various contributions were described by three structural parameters $N_{Ge\text{-}\xi}$ (number of ξ-type neighbors), $R_{Ge\text{-}\xi}$ (bond length), and $\sigma^2_{Ge\text{-}\xi}$ (Debye-Waller factor); the $N_{Ge\text{-}Ge}$ parameter, being related to Ge in the tetrahedral structure, was defined as $4\text{-}N_{Ge\text{-}Si}$. In order to reduce the total number of free parameters in the fit of the samples a preliminary analysis of the model compounds (crystalline Ge, Ge diluted in Si, and GeO_2) was carried out: from each fit the values of edge shift ΔE_0, the amplitude reduction factor S_0^2 and the Debye-Waller factors σ^2 for the first shell Ge-Ge, Ge-Si, and Ge-O were determined and used as fixed parameters during the sample modeling. The results of the quantitative analysis have been reported in Table I.

For comparison with the XPS/AFM results, in Fig. 4 we reported the average composition as determined by the XAS (solid squares) technique assuming a random distribution of the alloyed species within the Ge(Si) island layer,[12] i.e., $x = N_{Ge\text{-}Ge}/4$.

It is found that the average Ge content x decreases from $x=0.55$ down to $x=0.25$ upon increasing the silicon deposited thickness in the range $\theta_{Si} < 7.5$ nm. In this range the compositions determined by XAS are in good agreement with those obtained by means of the XPS/AFM technique. Given the different sampling depth of the two techniques, these results suggest that, in our experimental conditions, the island layer composition is quite homogeneous, as assumed in the XPS/AFM model.[5] XAS analysis also shows that for thicker Si deposition the Ge content inside the island layer does not change further.

TABLE I. Results of the quantitative XAS analysis. Errors were calculated as the square roots of the diagonal elements of the correlation matrix and are indicated in parentheses, when not indicated the parameter was kept fixed during the fit. For samples with $\theta_{Si}=0$ and 1 nm a Ge-O shell was needed to account for the oxidized phase. The oxide fraction results are, respectively, 37±7% and 27±7% and the observed Ge-O bond length, $R_{Ge\text{-}O}=1.74\pm0.01$ Å, typical of tetrahedrally coordinated Ge.

θ_{Si} (nm)	$N_{Ge\text{-}Si}$	$R_{Ge\text{-}Si}$ (Å)	$\sigma^2_{Ge\text{-}Si}$ (Å^2)	$R_{Ge\text{-}Ge}$ (Å)	$\sigma^2_{Ge\text{-}Ge}$ (Å^2)
Ge bulk	0	⋯	⋯	2.451(1)	30(1)
0	1.8(2)	2.39(1)	28	2.45(1)	64(6)
1	2.4(2)	2.38(1)	28	2.44(1)	57(8)
1.5	2.4(2)	2.38(2)	28	2.42(1)	30
4.5	2.5(1)	2.38(1)	28	2.441(3)	30
7.5	3.1(1)	2.385(6)	28	2.419(5)	30
18	2.9(2)	2.38(1)	28	2.428(6)	30
33	2.9(2)	2.38(1)	28	2.443(5)	30
Ge:Si	4.0(2)	2.381(3)	28(3)	⋯	⋯

DISCUSSION

Referring to Fig. 4, it is clear that the average Ge content x of the island layer decreases upon increasing the silicon thickness up to $\theta_{Si}=7.5$ nm, directly confirming that the driving mechanism of the morphological evolution observed in Figs. 1 and 2 is the Ge-Si intermixing upon Si deposition. This can be understood if we consider that the added silicon atoms help to reduce the system energy by diffusing into the islands and relaxing the island strain through enhanced alloying. This strain reduction allows the island to evolve toward a low-aspect ratio shape in order to reduce the surface energy. The Ge atoms close to the top of the strained domes serve as a reservoir for the Ge-Si intermixing, which takes place close to the surface. This Ge rearrangement, promoted by the newly arriving Si atoms, drives the island-shape transformation toward the (105)-bounded pyramid more stable configuration [as seen in the AFM data Fig. 1(a)–1(d)].

The simultaneous determination of the island layer morphology and composition allows us to discuss the island shape stability during the capping process in the $0\leqslant\theta_{Si}\leqslant4.5$ nm range, i.e., before the island burying. According to Rastelli *et al.*[9] the island shape (i.e., dome, pyramid or prepyramids) is uniquely determined by its volume and its average composition. As a consequence a phase diagram such as that reported in Fig. 7 can be constructed, where the two lines delimit the existence regions for domes, pyramids and prepyramids. Given that the island sizes scale as the square of the misfit,[6] the composition-dependent critical volume for the dome-to-pyramid transition (solid line) and the pyramid-to-prepyramid transition (dotted line) can be written as $V_C^{D,P}=V_0^{D,P}\times x^{-6}$ and $V_C^{P,PP}=V_0^{P,PP}\times x^{-6}$, respectively. $V_0^{D,P}$ was determined from the value of $V_C^{D,P}=9000$ nm^3 at $x=0.8$, which was measured in Ref. 20. The critical volume for the pyramid-to-prepyramid transition in the pure Ge/Si system ($x=1$) has been taken from Ref. 9 as $V_C^{P,PP}$ $(x=1)$ $=100$ nm^3.

The experimental points we reported in Fig. 7 have coordinates given by the measured average Ge contents and island volumes. Owing to the fact that shape and size distributions in our samples are monomodal (given the disappearance of the few uncapped pyramids constituting about the 5% of the overall measured initial island volume, see Figs. 1 and 2), the data illustrate the evolution of a typical island under Si deposition.

The observed evolution is in perfect agreement with the stability diagram. When the island volume drops below the composition dependent critical volume, a morphological change occurs leading to a reverse Stranski-Krastanov dynamics, i.e., an island shape evolution from high-aspect-ratio domes to low-aspect-ratio pyramids and prepyramids.[9] The experimental point above the *D-P* line corresponds to the uncapped sample. The incorporation of a little amount of silicon is therefore enough to drive the shape transition from domelike towards the more stable pyramids. By increasing the exposure to the Si flux the island shape evolves toward the *PP* stability region. At $\theta_{Si}=4.5$ nm, where we can still identify a pyramidal shape, the experimental points approach the *P-PP* stability line.

We found [Fig. 2(b)] that the island volume changes slightly throughout the entire evolution. The variation is much smaller than expected if one assumes that the islands

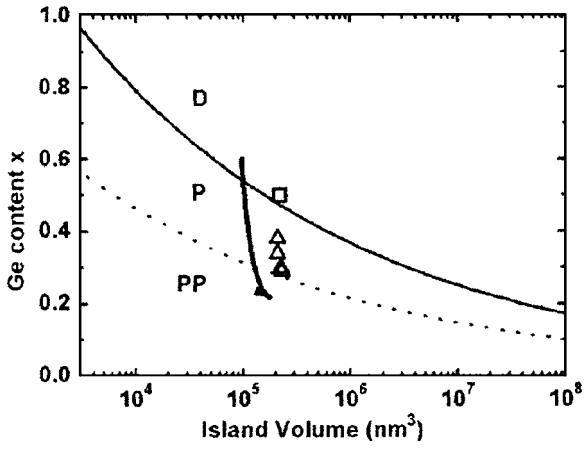

FIG. 7. Stability plot of the island shape as a function of the measured average composition and average volume in samples capped with increasing amount of silicon. The arrow indicates the evolution as the silicon equivalent thickness increases from $\theta_{Si}=0$ to $\theta_{Si}=4.5$ nm. The square represents a domelike shape whereas the triangles a pyramidlike shape as derived by AFM measurements. The critical volume for the morphological transition dome-to-pyramid (solid line) and pyramid-to-prepyramid (dotted line) are also displayed.

incorporate the silicon adatoms impinging over their projected area. As a consequence, one has to assume that the wetting layer and the islands behave as a single thermodynamic system in which the material can be redistributed in order to reduce the system free energy. For instance, an increase of the wetting layer thickness, due to surface/strain energy minimization, can result in an incorporation of the island edges into the wetting layer itself, resulting in an increase of the island volume slower than that predicted in Ref. 9. Furthermore, strain-driven adatom diffusion can be expected due to the nonuniform strain distribution.[29] For this reason, we remark here that an independent measurement of the average volume and composition is needed to build up the experimental stability diagram.

A further evolution of the islands towards mesa-shaped islands and eventually into more "rounded" island shape as observed in Fig. 1(e) ($\theta_{Si}=7.5$ nm) occurs while crossing the *P-PP* stability line. XPS measurements evidence (Fig. 3) that, at this stage of the overgrowth, the burial of the islands begins, with a thin silicon layer covering the entire surface. The higher Si surface energy can further promote the decay of the (105) facets into the (001) on the island top and to a rounded island shape, as suggested by Sutter *et al.*[30] Now the island shape is like the mesa shape we observed by means of cross-sectional transmission electron microscopy (XTEM) in Ge/Si(100) island multilayers grown in the same conditions.[31] The XTEM-measured average island height was about $h_{av}=10$ nm while we presently find an average height of $h_{av}=5$ nm for the mesalike islands. This discrepancy, together with the sudden decrease of the average island volume, evidences a nonconformal silicon growth at this stage with a higher growth rate in the region between the islands which brings about a progressive flattening of the surface. Interestingly this change in the growth mode is observed once the SiGe intermixing inside the islands has ended, as seen in Fig. 4 where the Ge content levels out at roughly $x=0.28$ for $\theta_{Si}=7.5$ nm. This saturation x value coincides with the critical alloy fraction for surface melting of Ge_xSi_{1-x} islands on Si(100) induced by the epitaxial strain at 750 °C as calculated by Bottomley.[32] Once this alloy fraction is reached, the mass transport on the surface is inhibited. A further flattening of the island, that requires additional silicon diffusing into the island itself,[30] is therefore inhibited: the island shape is now stabilized and the supplied silicon begins to form a capping layer.

We finally remark that XAS measurements indicate that the average composition of the *completely* buried islands does not depend on the amount of silicon coverage. This behavior can be attributed to the relatively higher bulk diffusion activation energy at 750 °C in SiGe multilayer upon strain relaxation[33] and evidences the stability of Ge island multilayer grown at high temperature. This property is very important in view of the integration of Ge-island-based optoelectronic devices into the standard CMOS-foundry process that requires high temperatures cycles ($T>700$ °C, e.g., for implant activation, salicide formation, etc.).

CONCLUSIONS

In this paper we discussed the effect of the deposition of a Si cap layer on the composition and morphological properties of Ge(Si)/Si(001) self-assembled islands deposited by UHV-CVD at 750 °C. The morphological evolution of the island shape was investigated by means of AFM and the actual composition of the island has been measured by means of XPS and XAS techniques. The data allowed us to define two regimes. For lower Si equivalent thickness (<7.5 nm) the deposited silicon is mainly incorporated in to the Ge(Si) islands. As proven by the measured island densities, at this stage the domes transform in pyramids and then in prepyramids while preexisting pyramids are either incorporated in larger islands or dissolved. The shape transition occurs through a redistribution of the Ge atoms from the island top to the side facets in order to reduce the system surface energy. The observed island shape evolution follows a reverse Stranski-Krastanov island growth dynamics in quantitative agreement with the island volume-composition stability diagram proposed for domes, pyramids and prepyramids in the Ge_xSi_{1-x}/Si(100) system.

Further silicon deposition entails silicon termination of the island facets and the destabilization of the facet orientation, promoting a rounded-mesalike island shape. Then, the silicon overgrowth proceeds in a nonconformal way leading to the complete burial of the islands and, eventually, to a flat sample surface growing in a layer-by-layer mode. The Ge average composition reaches the value $x=0.28$ before island burying and does not change for thicker cap layer. This behavior supports the conclusion that strain relief, rather than thermal diffusion, is the main driving force for the observed Ge-Si alloying.

[1] J. Stangl, V. Holý, and G. Bauer, Rev. Mod. Phys. **76**, 725 (2004).
[2] C. B. Li, R. W. Mao, Y. H. Zuo, L. Zhao, W. H. Shi, L. P. Luo, B. W. Cheng, J. Z. Yu, and Q. M. Wang, Appl. Phys. Lett. **85**, 2697 (2004).
[3] S. Tong, F. Liu, A. Khitun, K. L. Wang, and J. L. Liu, J. Appl. Phys. **96**, 773 (2004).
[4] I. Yakimov, A. V. Dvurechenskii, V. V. Kirienko, and A. I. Nikiforov, Appl. Phys. Lett. **80**, 4783 (2002).
[5] G. Capellini, M. De Seta, and F. Evangelisti, Appl. Phys. Lett. **78**, 303 (2001).
[6] M. De Seta, G. Capellini, F. Evangelisti, and C. Spinella, J. Appl. Phys. **92**, 614 (2002).
[7] O. G. Schmidt, U. Denker, S. Christiansen, and F. Ernst, Appl. Phys. Lett. **81**, 2614 (2002).
[8] A. Rastelli, E. Müller, and H. von Känel, Appl. Phys. Lett. **80**, 1438 (2002).
[9] A. Rastelli, M. Kummer, and H. von Känel, Phys. Rev. Lett. **87**, 256101 (2001).
[10] J. Cui, Q. He, X. M. Jiang, Y. L. Fan, X. J. Yang, F. Xue, and Z. M. Jiang, Appl. Phys. Lett. **83**, 2907 (2003).
[11] S. W. Lee, L. J. Chen, P. S. Chen, M.-J. Tsai, C. W. Liu, T. Y. Chien, and C. T. Chia, Appl. Phys. Lett. **83**, 5283 (2003).
[12] F. Boscherini, G. Capellini, L. Di Gaspare, F. Rosei, N. Motta, and S. Mobilio, Appl. Phys. Lett. **76**, 682 (2000).
[13] S. Wei, H. Oyanagi, K. Sakamoto, Y. Takeda, T. P. Pearsall, Phys. Rev. B **62**, 1883 (2000).
[14] P. Aebi, T. Tyliszczak, A. P. Hitchcock, K. M. Baines, T. K. Sham, Phys. Rev. B **45**, 13579 (1992).
[15] F. d'Acapito, P. Castrucci, N. Pinto, R. Gunnella, M. de Crescenzi, I. Davoli, Surf. Sci. **518**, 183 (2002).
[16] P. A. Lee, P. H. Citrin, P. Eisenberger, and B. M. Kincaid, Rev. Mod. Phys. **53**, 769 (1981).
[17] http://www.esrf.fr/exp_facilities/BM8/handbook/control.html

[18]S. Pascarelli, F. Boscherini, F. d'Acapito, J. Hrdy, C. Meneghini, and S. Mobilio, J. Synchrotron Radiat. **3**, 147 (1996).
[19]http://ixs.csrri.iit.edu/database/
[20]G. Capellini, M. De Seta, and F. Evangelisti, J. Appl. Phys. **93**, 291 (2003).
[21]S. A. Chaparro, Y. Zhang, J. Drucker, D. Chandrasekhar, and D. J. Smith, J. Appl. Phys. **87**, 2245 (2000).
[22]D. B. Migas, P. Raiteri, Leo. Miglio, A. Rastelli, and H. von Känel, Phys. Rev. B **69**, 235318 (2004).
[23]Ph. Sonnet and P. C. Kelires, Appl. Phys. Lett. **85**, 203 (2004).
[24]J. J. Rehr and R. C. Albers, Rev. Mod. Phys. **72**, 621–654 (2000).
[25]A. Ankudinov, B. Ravel, J. Rehr, and S. Conradson, Phys. Rev. B **58**, 7565 (1998).
[26]M. Newville, J. Synchrotron Radiat. **8**, 322 (2001).
[27]J. Glinnemann, H. E. King Jr., H. Schulz, T. Hahn, S. J. la Placa, and F. Dacol, Z. Kristallogr. **198**, 177 (1992).
[28]R. M. Martin, Phys. Rev. B **1**, 4005 (1970).
[29]A. van de Walle, M. Asta, and P. W. Voorhees, Phys. Rev. B **67**, 041308 (2003).
[30]P. Sutter and M. G. Lagally, Phys. Rev. Lett. **81**, 3471 (1998).
[31]G. Capellini, M. De Seta, C. Spinella, and F. Evangelisti, Appl. Phys. Lett. **82**, 1772 (2003).
[32]D. J. Bottomley, Appl. Phys. Lett. **79**, 1060 (2001).
[33]J.-M. Baribeau, R. Pascual, and S. Saimoto, Appl. Phys. Lett. **57**, 1502 (1990).